Earth Planets Space, **59**, 209–219, 2007

Envelope syntheses of cylindrical vector-waves in 2-D random elastic media based on the Markov approximation

Haruo Sato[1] and Michael Korn[2]

[1]*Department of Geophysics, Graduate School of Science, Tohoku University, Aramaki-Aza-Aoba 6-3, Aoba-ku, Sendai-shi, Miyagi-ken, 980-8578, Japan*
[2]*Institute of Geophysics and Geology, University of Leipzig, Talstrasse 35, 04103 Leipzig, Germany*

(Received May 11, 2006; Revised November 2, 2006; Accepted December 4, 2006; Online published May 7, 2007)

Seismograms of microearthquakes are complex; however, their envelopes broaden as the travel distance increases. P-waves are recorded in transverse components, S-waves are recorded in the longitudinal component, and waves are observed at sites even in the nodal direction of the source radiation. These phenomena, which are typically found in short-period seismograms, can be interpreted to be the result of scattering due to lithospheric inhomogeneity. We report here our study of a simple statistical model in which the propagation of waves radiated from a point source in two-dimensional (2-D) random elastic media is characterized by a Gaussian autocorrelation function. For the case that the wavelength is shorter than the correlation distance, two methods based on the Markov approximation are introduced for the direct synthesis of vector wave envelopes. One is to analytically solve the stochastic equation for the two-frequency mutual coherence function; the validity of the solution is confirmed by using finite difference simulations. The second is to numerically solve the stochastic equation for the mutual coherence function. The two methods are equivalent, but the latter is applicable to nonisotropic source radiation. For the case of a point shear dislocation source, a peak delay from the onset and a smoothly decaying tail are found to be common to synthesized envelopes in all azimuths. Scattered waves are excited even at receivers in the nodal direction, and amplitudes become independent of the radiation pattern as lapse time increases.

Key words: Scattering, random media, envelope, simulation.

1. Introduction

Seismic observations of local microearthquakes have revealed that high-frequency seismograms are strongly deformed by the propagation process through the randomly inhomogeneous structure of the lithosphere. In addition to the excitation of coda waves (Aki and Chouet, 1975), P-waves are seen in transverse components, S-waves are also seen in the longitudinal component (Matsumura and Sato, 1981), and waves are observed at sites even in the nodal direction of source radiation. Peak delay and the broadening of the envelope with increasing travel distance are also direct evidence of wave scattering due to medium inhomogeneity (Sato, 1989).

There have been developments in the modeling of wave envelopes in random media and analysis of observed seismogram envelopes (see Sato and Fehler, 1998). Complex waveforms have been deterministically and numerically simulated in inhomogeneous media (Frankel and Clayton, 1986; Yomogida and Benites, 1995). On the other hand, the radiative transfer theory with the statistical characterization of medium inhomogeneity has been often used as the basic framework of the envelope synthesis of high-frequency seismograms. Most of these studies treat energy propagation focusing on the coda portion of seismogram envelopes with the assumption of isotropic scattering (Sato, 1977; Zeng *et al*., 1993). Sato *et al*. (1997) provided an exact solution to the radiative transfer equation for isotropic scattering and a point shear dislocation source. This solution has been used in the inversion of strong motion records for the high-frequency radiation from an earthquake fault (see Nakahara *et al*., 1998); however, isotropic scattering assumption is not suitable for the envelope near the direct arrival where strong forward scattering dominates. There have been attempts to synthesize polarized vector wave envelopes, including the studies of Bal and Moscoso (2000), who analyzed the depolarization of S-waves after multiple scattering, and of Margerin *et al*. (2000), who synthesized envelopes by using scattering amplitudes of spherical inclusions distributed in uniform media and Stokes vectors. The radiative transfer theory is heuristic, but some studies have introduced scattering coefficients predicted from velocity inhomogeneity spectrum by using the Born approximation. Sato (1984) simulated three-component envelopes in random elastic media for a point shear dislocation source in the framework of single scattering approximation. Gusev and Abubakirov (1996) studied how the degree of nonisotropic scattering affects envelope shape. Recently, Przybilla *et al*. (2006) showed an excellent coincidence of envelopes synthesized by using the Monte Carlo method for the radiative transfer theory and those calculated from finite difference simulations in two-dimension (2-D) random elastic media.

These researchers used scattering amplitudes derived from the Born approximation with the wandering effect of travel time.

When the wavelength is smaller than the characteristic scale of medium inhomogeneity, conversion scattering is weak and scattering occurs around the forward direction, where the parabolic approximation is suitable for the synthesis of waves near the direct arrival. In this case, envelopes in random media can be well synthesized by the Markov approximation for the two-frequency mutual coherence function (TFMCF), which is a stochastic extension of the phase screen method (Ishimaru, 1978). Sato (1989) applied its solution for the interpretation of envelope broadening of observed S-wave seismograms in Kanto, Japan. Saito *et al*. (2002) theoretically solved the envelope broadening of spherically outgoing waves in von Kármán-type 3-D random media that have a realistic power-law spectrum at large wavenumbers. Fehler *et al*. (2000) confirmed the validity of the Markov approximation for scalar waves from a comparison with finite difference simulations in 2-D random media. Wegler *et al*. (2006) numerically examined the applicable range of the Markov approximation, and the radiative transfer solution with Born scattering amplitudes and that with isotropic scattering for scalar waves taking the finite difference simulation envelope as a reference in 2-D random media. Compared with the radiative transfer theory with Born scattering amplitudes, the Markov approximation method can not explain conversion scattering; however, if we focus on wave envelopes near the direct arrival, this approximation has the advantage that the envelope characteristics can be well described by a small number of statistical parameters. Extension of the Markov approximation to vector wave envelopes has been carried out recently by Korn and Sato (2005) and Sato (2006, 2007), who established a rigorous derivation of vector wave envelopes in random elastic media characterized by a Gaussian autocorrelation function (ACF) that uses the TFMCF of potential field. The validity of the Markov approximation for vector waves was confirmed from a comparison with finite difference simulations only for plane wave envelopes in the 2-D case (Korn and Sato, 2005).

There is yet another envelope synthesis, called the stochastic ray path method (Williamson, 1972, 1975), which is based on the joint use of the Markov approximation for the mutual coherence function (MCF) and ray travel times. The Monte Carlo method commonly used for the envelope simulation based on the radiative transfer theory treats travel distance and scattering angle as stochastic processes (Hoshiba, 1994; Yoshimoto, 2000). In contrast, the stochastic ray path method treats ray bending angle as a stochastic process and interprets the distribution of the accumulated travel times arriving at a given distance as the time trace of wave intensity. This method has the advantage that it is easily applicable to nonisotropic source radiation. In addition, it needs a relatively small number of shots for a stable estimation of envelopes compared with the conventional Monte Carlo method based on the radiative transfer theory.

In this paper, we report the results of a basic study of vector seismograms of micro-earthquakes in the lithospheric inhomogeneity. To this end, we mathematically simulate vector-wave envelopes for a point source radiation in 2-D random elastic media characterized by a Gaussian ACF. Using the Markov approximation for the TFMCF of potential, we solve vector wave envelopes for isotropic radiation from a point source. The synthesized envelopes are then compared with the ensemble-averaged envelopes of finite difference simulations. Next, using the Markov approximation for the MCF of potential, we derive the stochastic master equation appropriate for cylindrical waves. Using the stochastic ray path method—that is, numerically solving this equation and using ray travel times—we synthesize vector wave envelopes. The equality of two simulation methods of the Markov approximation is numerically confirmed for the case of isotropic radiation from a point source. Finally, applying the stochastic ray path method to the radiation from a point shear dislocation source, we synthesize vector wave envelopes at receivers in different azimuths.

2. Markov Approximation for the Two-Frequency Mutual Coherence Function

2.1 Two-frequency mutual coherence function

Wave propagation through 2-D inhomogeneous elastic media is studied in the case that the velocity inhomogeneity is small and the wavelength is shorter than the characteristic scale of inhomogeneity a. The spatial derivative of wave velocity can then be neglected, and the conversion scattering between the P- and S-waves is very small. The potential field $\phi\,(x, z, t)$ is governed by the wave equation in Cartesian coordinates (x, z),

$$\left(\partial_x^2 + \partial_z^2\right)\phi - \frac{1}{V_0^2}\partial_t^2\phi + \frac{2\xi}{V_0^2}\partial_t^2\phi = 0, \tag{1}$$

where $\xi\,(\mathbf{x})$ is fractional velocity fluctuation around the average velocity V_0.

We study the propagation of waves isotropically radiated from a point source located at the origin. At a distance r from the origin, which is larger than the wavelength ($r \gg 1/k_0$) and correlation distance ($r \gg a$), we may write outgoing waves as a sum of harmonic cylindrical waves of angular frequency ω using polar coordinates (r, θ) as

$$\phi\,(r, \theta, t) = \frac{1}{2\pi}\int_{-\infty}^{\infty} d\omega \frac{U\,(r, \theta, \omega)}{ik_0\sqrt{r}} e^{i(k_0 r - \omega t)}, \tag{2}$$

where θ is the polar angle measured from the z-axis and $k_0 = \omega/V_0$ is the wave number. Substituting Eq. (2) into Eq. (1), we obtain the parabolic wave equation for U as

$$2ik_0\partial_r U + \frac{\partial_\theta^2 U}{r^2} - 2k_0^2\xi U = 0, \tag{3}$$

where we neglect both a second derivative term with respect to radius since $a \gg 1/k_0$ and a term proportional to the inverse square of distance since $r \gg 1/k_0$.

We imagine an ensemble of fractional fluctuations $\{\xi\}$, where $\xi(\mathbf{x})$ is assumed to be a statistically homogeneous and isotropic random function of space coordinate $\mathbf{x}$. Here

we suppose that the randomness is statistically characterized by a Gaussian ACF $R(\mathbf{x}) \equiv \langle \xi(\mathbf{x}')\xi(\mathbf{x}'+\mathbf{x})\rangle = \varepsilon^2 \exp[-|\mathbf{x}|^2/a^2]$, where angular brackets represent the average over the ensemble. Parameters ε and a are root mean square (RMS) fractional fluctuation and correlation distance, respectively. The mean velocity is given by $V_0 = \langle V(\mathbf{x})\rangle$ since $\langle \xi(\mathbf{x})\rangle = 0$.

According to Fehler *et al*. (2000), we first define the TFMCF as the correlation of field U between two locations $r\theta'$ and $r\theta''$ within a small distance from the global ray direction θ=0 on the transverse line at distance r at different angular frequencies ω' and ω'', $\Gamma_2(r,\theta',\theta'',\omega',\omega'') \equiv \langle U(r,\theta',\omega')U(r,\theta'',\omega'')^*\rangle$. For quasi-monochromatic waves of central wavenumber $k_c = (k_0' + k_0'')/2$ and difference wavenumber $k_d = k_0' - k_0''$, we use the stochastic average of the parabolic wave Eq. (3) to obtain the master equation for TFMCF as

$$\partial_r \Gamma_2 + i\frac{k_d}{2k_c^2 r^2}\partial_{\theta_d}^2 \Gamma_2 + k_c^2 \left[A(0) - A(r\theta_d)\right]\Gamma_2 + \frac{k_d^2}{2}A(0)\,\Gamma_2 = 0, \tag{4}$$

where back scattering is neglected and causality is used for the derivation. This is called the Markov approximation. We used $\partial_{\theta'}^2\Gamma_2 = \partial_{\theta''}^2\Gamma_2 = \partial_{\theta_d}^2\Gamma_2$ since Γ_2 depends only on the difference angle between two locations $\theta_d = \theta' - \theta''$ and is independent of the center of mass angle $\theta_c = (\theta'+\theta'')/2$ because of the homogeneity of randomness and the isotropic radiation. The second term in Eq. (4) gives the ray propagation in the background homogeneous media, and the third term represents the interaction with medium inhomogeneity. Function A in Eq. (4) is the longitudinal integral of ACF as a function of difference transverse distance $x_d = r\theta_d$:

$$\begin{aligned} A(x_d) &\equiv \int_{-\infty}^{\infty} R(z, x_d)\,dz = \sqrt{\pi}\varepsilon^2 a e^{-\frac{x_d^2}{a^2}} \\ &\approx \sqrt{\pi}\varepsilon^2 a\left[1 - \frac{x_d^2}{a^2}\right] \quad \text{for} \quad |x_d| \ll a. \end{aligned} \tag{5}$$

At a long travel distance, the dominant contribution originates from the small transverse distance only. Factorizing Γ_2 into the product of ${}_0\Gamma_2$ and an exponential term as

$$\Gamma_2 = {}_0\Gamma_2 e^{-\frac{\omega_d^2 A(0) r}{2V_0^2}}, \tag{6}$$

we obtain the master equation for ${}_0\Gamma_2$:

$$\partial_r\, {}_0\Gamma_2 + i\frac{k_d}{2k_c^2 r^2}\partial_{\theta_d}^2\, {}_0\Gamma_2 + \frac{\sqrt{\pi}\varepsilon^2 k_c^2 r^2 \theta_d^2}{a}\,{}_0\Gamma_2 = 0. \tag{7}$$

Here we put the initial condition for a coherent impulsive isotropic radiation from a point source at the origin as

$$\Gamma_2(r \to 0, \theta_d, \omega_d, \omega_c) = {}_0\Gamma_2(r \to 0, \theta_d, \omega_d, \omega_c) = 1/(2\pi). \tag{8}$$

Fehler *et al*. (2000) analytically solved the master equation (7) under this initial condition as

$${}_0\Gamma_2(r, \theta_d, \omega_d, \omega_c) = \frac{1}{2\pi}\sqrt{\frac{s_0}{\sin s_0}}\, e^{-\left(\frac{1 - s_0 \cot s_0}{s_0^2}\right) 2V_0 r k_c^2 t_M \theta_d^2}, \tag{9}$$

Table 1. Assumptions and results.

Assumption	Result
Small fractional fluctuation $\varepsilon \ll 1$ and short wavelength $ak_0 \gg 1$	No conversion scattering. Parabolic equation for potential. Multiple small-angle scattering around the forward direction.
Ensemble of random media	Stochastic equation for field moments.
Causality and no backscattering	Markov-type stochastic master equation for TFMCF.
Long travel distance	Contribution comes from small transverse distances in A.
Type of random media: -Gaussian ACF -von Kármán-type ACF	Envelope width: -is independent of frequency. -increases with frequency.

where $s_0 = 2e^{\pi/4}\sqrt{t_M \omega_d}$ and the characteristic time $t_M = \sqrt{\pi}\varepsilon^2 r^2/(2V_0 a)$, which is practically independent of central angular frequency.

The Fourier transform of the exponential term in the RHS of Eq. (6) is

$$w(r,t) = \frac{1}{2\pi}\int_{-\infty}^{\infty} d\omega_d e^{-\frac{A(0)r}{2V_0^2}\omega_d^2} e^{-i\omega_d t} = \frac{V_0}{\sqrt{2\pi\sqrt{\pi}\varepsilon^2 a r}} e^{-\frac{V_0^2 t^2}{2\sqrt{\pi}\varepsilon^2 a r}}, \tag{10}$$

which does not influence the broadening of individual wave packets but shows the wandering effect from statistical averaging of the phase fluctuations of different rays. The time width of the wandering effect is proportional to the square root of travel distance. We note that $\lim_{r\to 0} w(r,t) = \delta(t)$ and $\int_{-\infty}^{\infty} w\,dt = 1$.

How each assumption affects the approximation and the results are summarized in Table 1.

2.2 Intensity spectral density

For P-waves, the angular-component intensity at a distance r is written as an integral of the intensity spectral density (ISD) $\widehat{I}_\theta^P$ over central angular frequency:

$$\begin{aligned} \left\langle \left|u_\theta^P(r,t)\right|^2 \right\rangle &= \left\langle \frac{\partial_{\theta'}\phi(r,\theta',t)}{r}\frac{\partial_{\theta''}\phi(r,\theta'',t)^*}{r}\right\rangle_{\theta'=\theta''} \\ &= \frac{1}{(2\pi)^2}\frac{1}{r}\int_{-\infty}^{\infty} d\omega' \int_{-\infty}^{\infty} d\omega'' \\ &\quad \cdot\left\langle \frac{\partial_{\theta'}U(r,\theta',\omega')}{k_0' r}\frac{\partial_{\theta''}U(r,\theta'',\omega'')^*}{k_0'' r}\right\rangle_{\theta'=\theta''} \\ &\quad \cdot e^{i(\omega'-\omega'')(t-r/V_0)} \\ &\approx \frac{1}{(2\pi)^2}\frac{1}{r}\int_{-\infty}^{\infty} d\omega_c \int_{-\infty}^{\infty} d\omega_d \\ &\quad \cdot\left[-\frac{1}{k_c^2 r^2}\partial_{\theta_d}^2\Gamma_2(r,\theta_d,\omega_d,\omega_c)\right]_{\theta_d=0} e^{-i\omega_d(t-r/V_0)} \\ &= \frac{1}{(2\pi)^2}\frac{1}{r}\int_{-\infty}^{\infty} d\omega_c \int_{-\infty}^{\infty} d\omega_d e^{-\frac{A(0)r}{2V_0^2}\omega_d^2} \\ &\quad \cdot\left[-\frac{1}{k_c^2 r^2}\partial_{\theta_d}{}_0^2\Gamma_2(r,\theta_d,\omega_d,\omega_c)\right]_{\theta_d=0} e^{-i\omega_d(t-r/V_0)} \\ &= \frac{1}{2\pi}\int_{-\infty}^{\infty} d\omega_c \widehat{I}_\theta^P(r,t;\omega_c), \end{aligned} \tag{11}$$

where we assumed that TFMCF is independent of θ_c. In a band with central angular frequency ω_c, and width Δf ($= \Delta\omega/2\pi$) and width $\widehat{I}^P_\theta$ the time trace of $\widehat{I}^P_\theta \Delta f$ gives the mean square (MS) envelope. ISD can be written as a convolution of ISD without wandering effect $\widehat{I}^P_{0\theta}$ and the wandering term w in time domain as

$$\widehat{I}^P_\theta\,(r,t;\omega_c) = \int_{-\infty}^{\infty} dt' w\left(r, t-t'\right) \widehat{I}^P_{0\theta}\left(r,t';\omega_c\right), \qquad (12)$$

where $\widehat{I}^P_{0\theta}$ is given by

$$\begin{aligned}
\widehat{I}^P_{0\theta}\,(r,t;\omega_c) &\equiv \frac{1}{2\pi r}\int_{-\infty}^{\infty} d\omega_d \left[-\frac{1}{k_c^2 r^2}\partial_{\theta_d}{}^2{}_0\Gamma_2\,(r,\theta_d,\omega_d,\omega_c)\right]_{\theta_d=0} \\
&\quad \cdot e^{-i\omega_d(t-r/V_0)} \\
&= \frac{1}{2\pi r}\frac{4V_0 t_M}{r}\frac{1}{2\pi}\int_{-\infty}^{\infty} d\omega_d \\
&\quad \cdot e^{-i\omega_d(t-r/V_0)}\frac{1-s_0\cot s_0}{s_0^2}\sqrt{\frac{s_0}{\sin s_0}} \\
&= \frac{4V_0}{r}\frac{1}{2\pi r}\frac{1}{2\pi}\int_{-\infty}^{\infty} d\omega_d e^{-i\omega_d(t-r/V_0)}\frac{\partial}{i\,\partial\omega_d}\sqrt{\frac{s_0}{\sin s_0}} \\
&= \frac{4V_0 t_M}{r}\frac{(t-r/V_0)}{t_M}\widehat{I}^R_0\,(r,t;\omega_c)\,. \qquad (13)
\end{aligned}$$

Here we define the reference ISD without wandering effect $\widehat{I}^R_0$ as the Fourier transform of ${}_0\Gamma_2$ as

$$\begin{aligned}
\widehat{I}^R_0\,(r,t;\omega_c) &= \frac{1}{2\pi r}\int_{-\infty}^{\infty} d\omega_d \\
&\quad \cdot{}_0\Gamma_2\,(r,\theta_d=0,\omega_d,\omega_c)\,e^{-i\omega_d(t-r/V_0)} \\
&= \frac{1}{2\pi r}\frac{1}{2\pi}\int_{-\infty}^{\infty} d\omega_d\sqrt{\frac{s_0}{\sin s_0}}e^{-i\omega_d(t-r/V_0)}, \qquad (14)
\end{aligned}$$

which is the ISD of a cylindrical scalar wave as derived in Fehler *et al.* (2000). For the derivation of the last line in Eq. (13) we used the relation $2\pi i u g\,(u) = \int_{-\infty}^{\infty} d\omega_d e^{-i\omega_d u}\partial_{\omega_d}\hat{g}\,(\omega_d)$, where $\hat{g}$ is the Fourier transform of time function g.

Using the leading term in Eq. (3), $\partial_r U \approx (i/2k_0 r^2)\partial_\theta^2 U$, we have the radial-component intensity as

$$\begin{aligned}
\left\langle \left|u^P_r\,(r,t)\right|^2\right\rangle &= \left\langle \partial_r\phi\left(r,\theta',t\right)\partial_r\phi\left(r,\theta'',t\right)^*\right\rangle_{\theta'=\theta''} \\
&= \frac{1}{(2\pi)^2}\frac{1}{r}\int_{-\infty}^{\infty} d\omega'\int_{-\infty}^{\infty} d\omega'' \\
&\quad \cdot\left\langle\left(U'+\frac{\partial_r U'}{ik_0'}\right)\left(U''+\frac{\partial_r U''}{ik_0''}\right)^*\right\rangle_{\theta'=\theta''} \\
&\quad \cdot e^{i\left(\omega'-\omega''\right)(t-r/V_0)} \\
&\approx \frac{1}{(2\pi)^2}\frac{1}{r}\int_{-\infty}^{\infty} d\omega'\int_{-\infty}^{\infty} d\omega'' \\
&\quad \cdot\left\langle U'U''a^* + \frac{\partial^2_{\theta'}U'}{2k_0'^2 r^2}U''^* + U'\frac{\partial^2_{\theta''}U''^*}{2k_0''^2 r^2}\right\rangle_{\theta'=\theta''} \\
&\quad \cdot e^{i\left(\omega'-\omega''\right)(t-r/V_0)} \\
&\approx \frac{1}{(2\pi)^2}\frac{1}{r}\int_{-\infty}^{\infty} d\omega_c\int_{-\infty}^{\infty} d\omega_d \\
&\quad \cdot\left[\left(1+\frac{1}{r^2k_c^2}\partial^2_{\theta_d}\right)\Gamma_2\,(r,\theta_d,\omega_d,\omega_c)\right]_{\theta_d=0} \\
&\quad \cdot e^{-i\omega_d(t-r/V_0)} \\
&= \frac{1}{(2\pi)^2}\frac{1}{r}\int_{-\infty}^{\infty} d\omega_c\int_{-\infty}^{\infty} d\omega_d e^{-\frac{A(0)r}{2V_0^2}\omega_d^2} \\
&\quad \cdot\left[\left(1+\frac{1}{r^2k_c^2}\partial^2_{\theta_d}\right){}_0\Gamma_2\,(r,\theta_d,\omega_d,\omega_c)\right]_{\theta_d=0} \\
&\quad \cdot e^{-i\omega_d(t-r/V_0)} \\
&= \frac{1}{2\pi}\int_{-\infty}^{\infty} d\omega_c \widehat{I}^P_r\,(r,t;\omega_c)\,, \qquad (15)
\end{aligned}$$

where the radial component ISD $\widehat{I}^P_r$ is written as a convolution of ISD without wandering effect $\widehat{I}^P_{0r}$ and the wandering term w as

$$\widehat{I}^P_r\,(r,t;\omega_c) = \int_{-\infty}^{\infty} dt' w\left(r,t-t'\right)\widehat{I}^P_{0r}\left(r,t';\omega_c\right). \qquad (16)$$

We note that $\widehat{I}^P_{0r}$ is written as

$$\begin{aligned}
\widehat{I}^P_{0r}\,(r,t;\omega_c) &= \frac{1}{2\pi r}\int_{-\infty}^{\infty} d\omega_d \\
&\quad \cdot\left[\left(1+\frac{1}{r^2k_c^2}\partial^2_{\theta_d}\right)_0\Gamma_2\,(r,\theta_d,\omega_d,\omega_c)\right]_{\theta_d=0} \\
&\quad \cdot e^{-i\omega_d(t-r/V_0)} \\
&= \widehat{I}^R_0\,(r,t;\omega_c) - \widehat{I}^P_{0\theta}\,(r,t;\omega_c) \qquad (17)
\end{aligned}$$

The initial condition of Eq. (8) represents the isotropic radiation of a wavelet characterized by a delta-fucntion for the source time function's square per frequency:

$$\begin{aligned}
&\widehat{I}^R_0\,(r,t;\omega_c) = \widehat{I}^P_{0r}\,(r,t;\omega_c) = \frac{1}{2\pi r}\delta\left(t-\frac{r}{V_0}\right) \\
&\text{and}\quad \widehat{I}^P_{0\theta}\,(r,t;\omega_c) = 0 \quad \text{as} \quad r\to 0. \qquad (18)
\end{aligned}$$

For a given source time function's square per angular frequency $i\,(t;\omega_c)$, we calculate the convolution $\widehat{I}^P_\theta \otimes i$ for the angular component and $\widehat{I}^P_r \otimes i$ for the radial component since constituent waves are incoherent.

For the case of isotropic radiation of an S-wavelet from a point source, replacing P with S and substituting the average S-wave velocity into V_0, $\widehat{I}^P_r$ and $\widehat{I}^P_\theta$ represent the angular and radial component wave intensities $\widehat{I}^S_\theta$ and $\widehat{I}^S_r$, respectively.

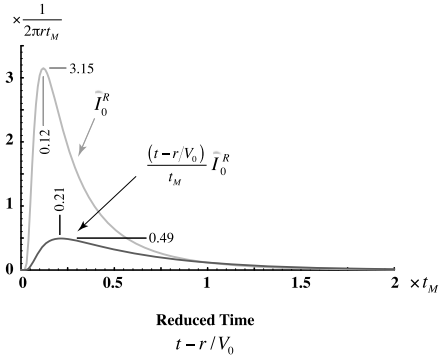

Fig. 1. Temporal change in $\widehat{I}_0^R$ and $(t - r/V_0)\,\widehat{I}_0^R/t_M$ against reduced time $t - r/V_0$ for a point source radiation in random elastic media characterized by a Gaussian ACF.

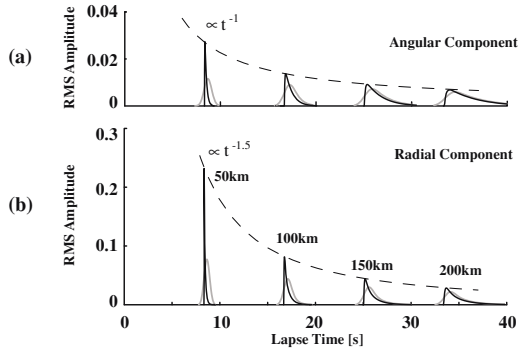

Fig. 2. Square root ISD envelopes of P-waves for an isotropic radiation from a point source in random elastic media characterized by a Gaussian ACF predicted by the Markov approximation for TFMCF: (a) the angular component and (b) the radial component. Thin solid curves and gray bold curves show square root of ISDs without wandering effect and those with wandering effect, where the source time function of a 2-Hz wavelet. Broken curves show peak amplitude decays according to a power of lapse time.

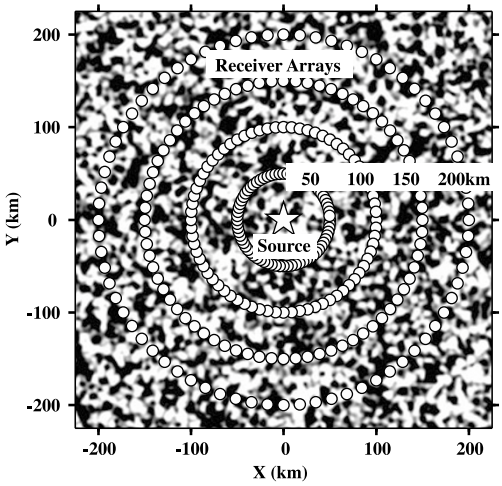

Fig. 3. Schematic illustration of one realization of a random elastic medium characterized by a Gaussian ACF ($\varepsilon = 5\%$ and $a = 5$ km) and the configuration of a source (star) and four receiver arrays (circles) used for FD numerical simulations, where mean P- and S-wave velocities are 6 km/s and 3.46 m/s, respectively.

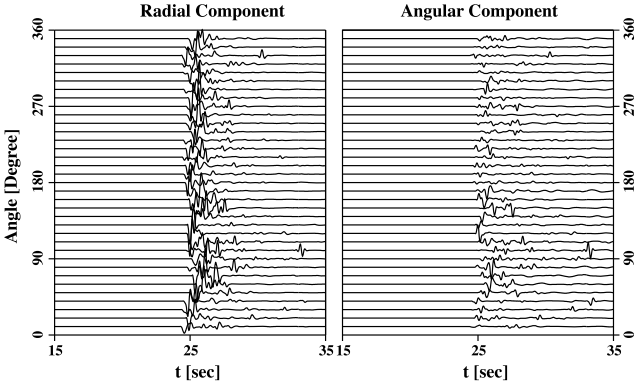

Fig. 4. Examples of FD simulation traces at a distance of 150 km in one realization of a random elastic medium characterized by the Gaussian ACF for the isotropic radiation of a 2-Hz P-wavelet from a point source. Only every second trace is plotted.

2.3 Characteristics of resultant ISDs

As was done in Fehler *et al.* (2000), we can numerically evaluate the reference ISD without wandering effect by Eq. (14) by using an Fast Fourier Transform (FFT). In Fig. 1 we plot $\widehat{I}_0^R$ as a gray curve against reduced time $t - r/V_0$. It takes the maximum value of about $3.15/(2\pi r t_M)$ at the reduced time of about $0.12t_M$. The peak height of $\widehat{I}_0^R$ is proportional to the inverse cube of travel distance since the characteristic time is proportional to the square of distance. A black curve shows $(t - r/V_0)\,\widehat{I}_0^R/t_M$, which has the maximum value of about $0.49/(2\pi r t_M)$ at the reduced time of about $0.21t_M$, which is nearly twice the peak delay of $\widehat{I}_0^R$. This means that $\widehat{I}_{0\theta}^P$ has a maximum value of about $0.31V_0/r^2$. The peak height of $\widehat{I}_{0\theta}^P$ is nearly proportional to the inverse cube of travel distance as $\widehat{I}_0^R$ when the peak height of $\widehat{I}_{0\theta}^P$ is negligible. There are constraints on the time integral of ISDs. We have $\int_{r/V_0}^{\infty} dt \widehat{I}_0^R = 1/(2\pi r)$; however, the time integral of $\widehat{I}_{0\theta}^P$ is independent of travel distance as $\int_{r/V_0}^{\infty} dt \widehat{I}_{0\theta}^P = \varepsilon^2/\left(3\sqrt{\pi}a\right)$, suggesting that the time integral of $\widehat{I}_{0\theta}^P$ offers a stable measure of the ratio of velocity inhomogeneity to the correlation distance.

In Fig. 2, we plot the time traces of square root ISDs, which is a more appropriate means for a comparison with RMS envelopes, where $\varepsilon = 5\%$ and $a = 5$ km and the average P-wave velocity is 6 km/s. We note that $\widehat{I}_{0\theta}^P$ exceeds $\widehat{I}_0^R$ as the reduced time increases, indicating a violation of the approximation. Theoretical curves are plotted only in the range of $\widehat{I}_{0\theta}^P < \widehat{I}_0^R$. The asymptotic peak decay curve of the angular component $\sqrt{\widehat{I}_{0\theta}^P}$ and that of the radial component $\sqrt{\widehat{I}_{0r}^P}$ are shown by power law curves t^{-1} and $t^{-1.5}$, respectively, as plotted by broken curves.

2.4 Comparison with finite-difference simulations

A standard finite difference technique in space-time domain is employed for the syntheses of vector waves in various realizations of 2-D random elastic media. The practical scheme is the same as that reported in Korn and Sato (2005), where the equations for particle velocities and stresses in an isotropic inhomogeneous elastic medium are solved on a staggered grid. The accuracy is second-order in time and

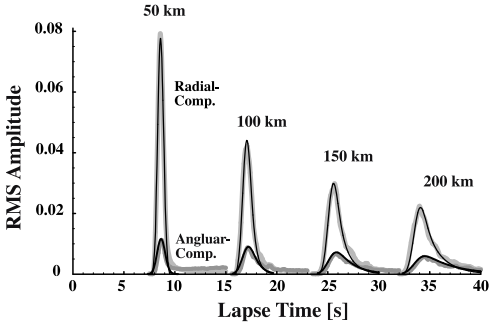

Fig. 5. Comparison of RMS envelopes of FD simulated waves (bold gray curves) and theoretical envelopes directly predicted by the Markov approximation (thin black curves) in random media characterized by a Gaussian ACF for the isotropic radiation of a 2-Hz P-wavelet from the point source.

fourth-order in space. Absorbing boundary conditions are implemented at the boundaries of the computational grid. The size of the model is 450×450 km, as illustrated in Fig. 3. In the following simulation, we used $\varepsilon = 5\%$ and $a = 5$ km. Mean P- and S-wave velocities are 6 km/s, and 3.46 km/s, respectively. The fractional fluctuation of mass density is chosen as 0.8ξ (**x**) according to Birch's law (see Sato, 1984). This model is scaled to be a representative of an average crust for high-frequency seismic wave propagation.

The far-field pulse shape of the outgoing P-wavelet in a homogenous medium radiated isotropically from a source located at the center is given by the convolution $u_r = g_2 \otimes h$, where the 2-D Green function $g_2(r,t) = 2V_0 H(V_0 t - r)/\sqrt{V_0^2 t^2 - r^2}$ (Morse and Feshbach, 1953, p. 842) is approximated as $g_2(r,t) \approx \sqrt{2}V_0/\sqrt{r\,(V_0 t - r)}$ near the wave front $t \approx r/V_0$. The source time function is given by

$$h(t) = c\left[\sin\frac{N\pi}{T}t - \frac{N}{N+2}\sin\frac{(N+2)\,\pi}{T}t\right] \quad \text{for} \quad 0 \le t \le T, \tag{19}$$

where T is the duration of the wavelet, and N is a parameter indicating the number of maxima and minima of the wavelet. Choosing $N = 2$ and $T = 0.5$ s, we have a 2-Hz wavelet with a band-limited spectrum of half-width Δf between 0.8 and 4.1 Hz. Around the source a homogeneous region of 1-km width is introduced to ensure pure isotropic P-wave radiation. Factor c in the source time function is chosen to satisfy $\int_0^T 2\pi r\ |u_r|^2\, dt = 1$ near the source.

The wave field is recorded at circular arrays of receivers at $r = 50$, 100, 150 and 200 km, respectively. Each circular array consists of 72 receivers at intervals of 5°, as shown by open circles in Fig. 3. The spatial discretization in the finite-difference (FD) scheme is 0.1 km, and the temporal discretization is 6 ms, slightly below the stability limit of the numerical scheme. This choice ensures that the numerical errors remain small. The wavelength of a 2-Hz P-wavelet is smaller than the correlation distance and the medium inhomogeneity is weak.

Figure 4 shows examples of FD waveforms that have travelled 150 km through one realization of random elastic medium. Strong distortions of pulse shape and travel time fluctuations are clearly seen. The P-wave is followed by scattered waves in the radial-component traces, and scattered waves also appear in the angular-component traces. We obtain the ensemble-averaged envelope at each travel distance by averaging the square of wave traces over 72 receivers along the circular array in five realizations of random media, smoothing with time constant 0.5 s, and taking the square root. The bold gray curves in Fig. 5 show RMS envelopes at four travel distances, clearly revealing that the peak delay and the time width of the envelope increase with travel distance—in both the radial and angular components. The existence of wave trains in the angular component provides clear evidence of scattering caused by random inhomogeneity. At each travel distance, the peak amplitude of the angular component is smaller than that of the radial component; however, the former amplitude decreases more slowly than that of the latter amplitude. The peak delay of the angular component looks larger than that of the radial component.

Using ISDs with wandering effect calculated from the Markov approximation for the same parameters characterizing random media, we perform the convolution with the source time function's square of the 2 Hz P-wavelet; then, taking square root $\sqrt{\widehat{I}_\theta^P \otimes i}$ and $\sqrt{\widehat{I}_r^P \otimes i}$, we obtain RMS envelopes, where we practically put $i(t) = 2\pi r\,|u_r|^2$ of the FD simulation near the source. Theoretical RMS envelopes according to the Markov approximation are shown by the plots of gray curves in Fig. 2. Each envelope has a longer time width and a smaller peak height compared with the corresponding envelope without wandering effect. We find that the difference becomes smaller as the travel distance increases. In Fig. 5, RMS envelopes $\sqrt{\widehat{I}_\theta^P \otimes i}$ and $\sqrt{\widehat{I}_r^P \otimes i}$ predicted by the Markov approximation are plotted as thin black curves together with FD envelopes. We find that the Markov approximation envelopes well explain the peak height, the delay of the peak arrival from the onset, and the envelope broadening of FD envelopes at four distances. We also find a small discrepancy between them as reduced time increases at each travel distance since FD envelopes contain large angle scattering and conversion scattering that the Markov approximation neglects. The importance of conversion scattering for P-coda is carefully examined by Przybilla *et al.* (2006). With the exception of the coda portion, FD envelopes are quantitatively well explained by Markov envelopes.

The time integral of FD envelopes $\int 2\pi r(|u_r|^2 + |u_\theta|^2)dt$ takes nearly the same value as that predicted from the Markov approximation at four distances and the relative error is less than 2%, where the time window length is chosen as 7, 12, 18, and 24 s at 50, 100, 150 and 200 km, respectively. The ratio of time integrals of FD envelopes $\int |u_\theta|^2 dt / \int 2\pi r(|u_r|^2 + |u_\theta|^2)dt$ is nearly equal to the predicted ratio $\varepsilon^2/(3\sqrt{\pi}a)$ with a relative error of less than 4%. These results show that the partition of the power into the angular component is a stable and reliable measure of randomness. Our results indicate that the predictions made by the Markov approximation are reliable for the case of velocity fractional fluctuation ε up

to 5%.

3. Stochastic Ray Path Method

We introduce a stochastic master equation for MCF of potential field on the basis of the Markov approximation. The stochastic ray path method of Williamson (1972) uses the solution of this stochastic equation with ray travel times for the evaluation of scalar wave envelope at a given travel distance. Extending this method to vector waves, we calculate vector component intensities for a point source radiation.

3.1 Markov approximation for the MCF

For waves isotropically radiated from a point source located at the origin, we define the MCF of field U between different locations on the transverse line (x-axis) at a large distance r as $\Gamma_1(r,\theta',\theta'',\omega) \equiv \langle U(r,\theta',\omega)U(r,\theta'',\omega)^*\rangle$. The MCF is a function of the difference transverse coordinate $x_d \equiv r\theta_d = r(\theta'-\theta'')$ since it is independent of the center of mass angle $\theta_c = (\theta'+\theta'')/2$ because of isotropy of randomness and isotropic source radiation. Neglecting backward scattering and using causality, we can derive the master equation for MCF according to the Markov approximation as

$$\partial_r \Gamma_1 + k_0^2 \left[A(0) - A(r\theta_d)\right]\Gamma_1 = 0, \tag{20}$$

where A is the longitudinal integral of ACF as defined by Eq. (5) (see p. 244, Sato and Fehler, 1998). Integrating Eq. (20) for an increment Δr, we have a solution of MCF at $r+\Delta r$ as

$$\Gamma_1(r+\Delta r, x_d, \omega) = e^{-k_0^2[A(0)-A(x_d)]\Delta r}\,\Gamma_1(r, x_d, \omega)\,. \tag{21}$$

Using Eq. (21) successively by a split step method with an increment Δr, we get Γ_1 at any distance r. The angular spectrum function (ASF) is defined as the Fourier transform of MCF in the transverse plane,

$$\breve{\Gamma}_1(r,k_x,\omega) = \int_{-\infty}^{\infty} dx_d e^{-ik_x x_d}\Gamma_1(r,x_d,\omega) \tag{22}$$

This gives the distribution of ray wavenumbers. We may write Eq. (21) as a convolution for ASF,

$$\breve{\Gamma}_1(r+\Delta r,k_x,\omega) = \frac{1}{2\pi}\int_{-\infty}^{\infty} dk_x' \breve{\Phi} \cdot\left(\Delta r, k_x - k_x', \omega\right)\breve{\Gamma}_1\left(r,k_x',\omega\right) \tag{23}$$

where the integral kernel is

$$\breve{\Phi}(\Delta r,k_x,\omega) = \int_{-\infty}^{\infty} dx_d e^{-ik_x x_d} e^{-k_0^2[A(0)-A(x_d)]\Delta r}. \tag{24}$$

The meaning of ASF becomes clear if we change the argument from wavenumber k_x to local ray angle $\phi \approx k_x/k_0$ in the case of small angle scattering. Replacing $\frac{k_0}{2\pi}\breve{\Gamma}_1(r,k_0\phi,\omega)$ with $\breve{\Gamma}_\phi(r,\phi,\omega)$, we re-define the ASF for ray angle ϕ. We may then write Eq. (23) as

$$\breve{\Gamma}_\phi(r+\Delta r,\phi,\omega) = \int_{-\infty}^{\infty} d\phi' \breve{\Phi}_\phi \cdot\left(\Delta r, \phi-\phi', \omega\right)\breve{\Gamma}_\phi\left(\phi',r,\omega\right), \tag{25}$$

where the transfer function for ϕ is

$$\breve{\Phi}_\phi(\Delta r,\phi,\omega) \equiv \frac{k_0}{2\pi}\breve{\Phi}(\Delta r, k_0\phi,\omega) = \frac{1}{2\pi}\int_{-\infty}^{\infty} dw e^{-i\phi w} e^{-k_0^2\left[A(0)-A\left(\frac{w}{k_0}\right)\right]\Delta r}, \tag{26}$$

which is normalized as $\int_{-\infty}^{\infty}\breve{\Phi}_\phi d\phi = 1$. Equation (26) means that ray bending process is essentially governed by the spectrum of random media through function A. Ray bending is small when the wavelength is shorter than the correlation distance and velocity fluctuation is small. As travel distance increases, the incoherent term controlled by the transfer function at a small transverse distance dominates over the coherent term. For the envelope synthesis at a long travel distance, it is enough to use the transfer function at a small transverse distance only (see, for example, Ishimaru, 1978, p. 321). For the case of Gaussian ACF, substituting Eq. (5) into Eq. (26), we have a Gaussian-type transfer function as

$$\breve{\Phi}_\phi(\Delta r,\phi,\omega) \approx \frac{1}{\sqrt{2\pi}\sqrt{\frac{2\sqrt{\pi}\varepsilon^2\Delta r}{a}}} e^{-\frac{\phi^2}{2\left(\frac{2\sqrt{\pi}\varepsilon^2\Delta r}{a}\right)}}, \tag{27}$$

where the standard deviation $\sqrt{2\sqrt{\pi}\varepsilon^2\Delta r/a}$ is independent of angular frequency.

Intensity in the angular-frequency domain is defined by the ensemble average of the Fourier transform of displacement vector $\hat{\mathbf{u}}^P(r,\omega)$. The angular component intensity in angular-frequency domain is given by

$$\begin{aligned}\widehat{J}_\theta^P(r;\omega) &\equiv \left\langle\left|\hat{u}_\theta^P(r,\omega)\right|^2\right\rangle \\ &= \left\langle \frac{\partial_{\theta'}U\left(r,\theta',\omega\right)}{r\,k_0\sqrt{r}}\frac{\partial_{\theta''}U\left(r,\theta'',\omega\right)^*}{r\,k_0\sqrt{r}}\right\rangle_{\theta'=\theta''} \\ &= \frac{1}{r}\left[-\frac{1}{k_0^2 r^2}\partial_{\theta_d}^2\Gamma_1(r,\theta_d,\omega)\right]_{\theta_d=0}.\end{aligned} \tag{28}$$

This can be written as an integral over local ray angle θ:

$$\begin{aligned}\widehat{J}_\theta^P(r;\omega) &= \frac{1}{r}\left[-\frac{1}{k_0^2}\partial_{x_d}^2\Gamma_1(r,x_d,\omega)\right]_{x_d=0} \\ &= \frac{1}{r}\left[\frac{1}{2\pi}\int_{-\infty}^{\infty} dk_x \frac{k_x^2}{k_0^2}\breve{\Gamma}_1(r,k_x,\omega)\right] \\ &\approx \frac{1}{r}\int_{-\infty}^{\infty} d\phi\phi^2\breve{\Gamma}_\phi(r,\phi,\omega)\,.\end{aligned} \tag{29}$$

The radial-component intensity in angular-frequency domain is given by

$$\begin{aligned}\widehat{J}_r^P(r;\omega) &\equiv \left\langle\left|\hat{u}_r^P(r,\omega)\right|^2\right\rangle \\ &\approx \frac{1}{r}\left[\left(1+\frac{1}{r^2k_0^2}\partial_{\theta_d}^2\right)\Gamma_1(r,\theta_d,\omega)\right]_{\theta_d=0},\end{aligned} \tag{30}$$

which is written as an integral over local ray angle ϕ:

$$\begin{aligned}\widehat{J}_r^P(r;\omega) &= \frac{1}{r}\left[\left(1+\frac{1}{k_0^2}\partial_{x_d}^2\right)\Gamma_1(r,x_d,\omega)\right]_{x_d=0} \\ &= \frac{1}{r}\left[\frac{1}{2\pi}\int_{-\infty}^{\infty} dk_x\left(1-\frac{k_x^2}{k_0^2}\right)\breve{\Gamma}_1(r,k_x,\omega)\right] \\ &\approx \frac{1}{r}\int_{-\infty}^{\infty} d\phi\left(1-\phi^2\right)\breve{\Gamma}_\phi(r,\phi,\omega)\,.\end{aligned} \tag{31}$$

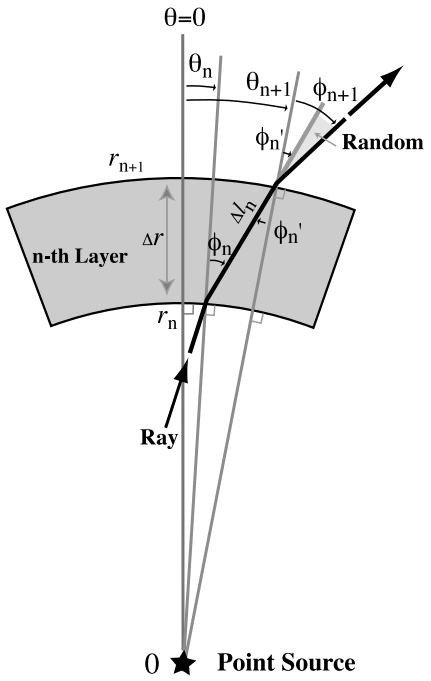

Fig. 6. Ray bending process through cylindrical layers with thickness Δr in an inhomogeneous random medium.

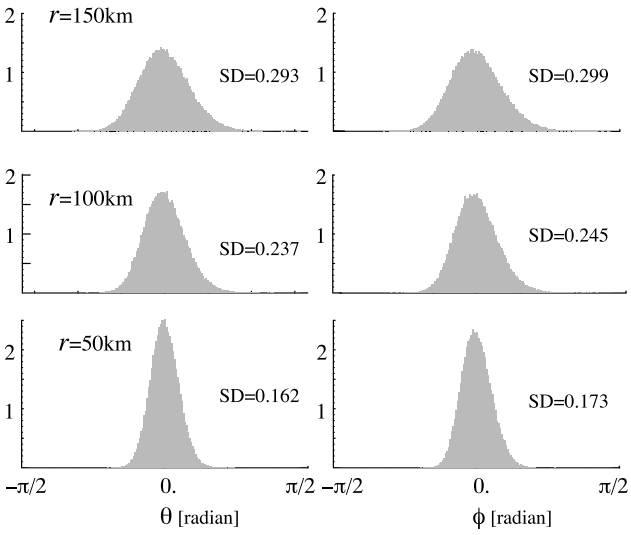

Fig. 7. Distribution of ray coordinate angle θ and that of local ray angle ϕ (ASF) at three distances. The initial ray direction is $\theta = 0$ and $\phi = 0$. SD means the standard deviation.

The isotropic radiation of coherent waves from the origin is written by the initial condition $\Gamma_1(r \to 0, x_d, \omega) = 1/(2\pi)$, that is, $\breve{\Gamma}_\phi(r \to 0, \phi, \omega) = \delta(\phi)/(2\pi)$. When the medium is homogeneous, $\widehat{J}_r^P(r\omega) = 1/(2\pi r)$ and $\widehat{J}_\theta^P(r\omega) = 0$. Once ASF $\breve{\Gamma}_\phi$ is obtained in random media, it is easy to calculate both radial and angular-component intensities $\widehat{J}_r^P$ and $\widehat{J}_\theta^P$ at a given distance from the point source. We should note that Eqs. (29) and (31) describe stationary state.

For the case of S-waves, replacing P with S in $\widehat{J}_r^P$ and $\widehat{J}_\theta^P$, we have the angular and radial-component wave intensities in angular-frequency domain, respectively.

3.2 Cylindrical layers and ray travel times

The split-step solution - Eq. (25) - describes how rays are bent according to the velocity inhomogeneity in a layer of thickness Δr for stationary state. Williamson (1972) interpreted the convolution integral equation Eq. (25) as a Wiener process in that the change in ray direction is stochastically controlled by the spectrum of random media through factor A. To extend the above solution to non-stationary state problem, he used the accumulated travel time for each ray path from a source to a receiver. He proposed this method for the synthesis of scalar wave envelopes for the case of the Gaussian transfer function. Williamson (1975) denoted this method as the stochastic ray path method, and a compact summary is given in Uscinski (1977, Chapter 6).

The ray bending process takes place in a small region which can be well described using local Cartesian coordinates; however, it is necessary to use polar coordinates to describe the ray trajectory from a point source located at the origin. As illustrated in Fig. 6, we divide a random medium into many cylindrical layers with a small thickness of Δr. At the n-th boundary, the absolute ray location is given by ray coordinates $(\theta_n,\ r_n)$, where r_n is the radius from the source, θ_n is the ray angle from the initial ray direction from the source $\theta = 0$, and local ray angle ϕ_n is measured from a radial direction from the source. At the $n+1$th boundary after an increment of radius Δr in the n-th layer, the ray coordinate becomes $(\theta_{n+1},\ r_{n+1})$, and the incident angle to the $n+1$th boundary is ϕ_n'. The path length Δl_n satisfies $\Delta l_n \sin\phi_n = r_{n+1}(\theta_{n+1} - \theta_n)$ and $\Delta l_n \sin\phi_n' = r_n(\theta_{n+1} - \theta_n)$; that is, $\sin\phi_n' / \sin\phi_n = r_n/(r_n + \Delta r)$. For a small local ray angle, we have $\phi_n' = r_n\phi_n/(r_n + \Delta r) \approx (1 - \Delta r/r_n)\phi_n$. The local ray angle at the $n+1$-th boundary is bent by the medium inhomogeneity as a stochastic process, which is written by

$$\phi_{n+1} = \phi_n' + Random \approx (1 - \Delta r/r_n)\phi_n + Random. \tag{32}$$

Random angles are practically generated by using the Monte Carlo method for the transfer function Eq. (27). The ray coordinate angle at the $n+1$-th boundary then becomes

$$\theta_{n+1} \approx \theta_n + (\Delta r/r_n)\phi_n. \tag{33}$$

When the travel time of this ray at the n-th boundary is t_n, the travel time at the $n+1$-th boundary becomes

$$t_{n+1} = t_n + \frac{\Delta l_n}{V_0} \approx t_n + \frac{\Delta r}{V_0}\left(1 + \frac{\phi_n^2}{2}\right). \tag{34}$$

For the synthesis of wave envelopes in the case of impulsive radiation from a point source, we shoot many particles from the origin to a fixed direction and calculate ASF with travel time distribution at a given receiver. We use integrals over ray angles (29) and (31) for the calculation of two vector component intensities. Since we calculate the travel time for each layer by using the average velocity V_0, the resultant travel time distribution gives intensity without wandering effect. If we need intensity with wandering effect, we just calculate the convolution of the intensity here

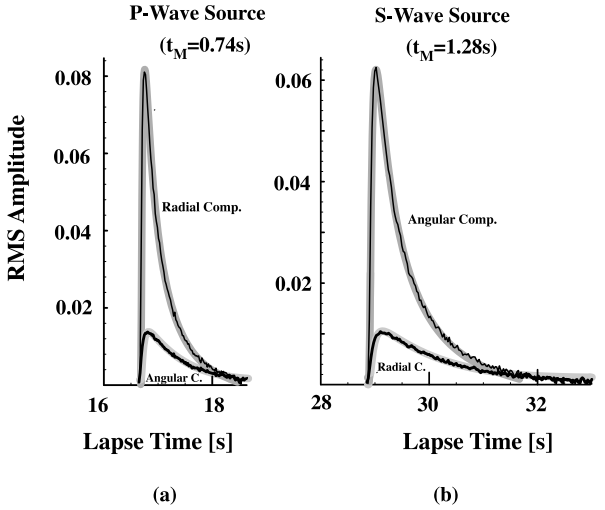

Fig. 8. Square root intensity envelopes at a distance of 100 km for isotropic radiation from a point source in 2-D random elastic media characterized by a Gaussian ACF: (a) P-wave case, (b) S-wave case. Comparison of the Markov approximation for TFMCF without wandering effect of (gray curves) and the stochastic ray path method (thin black curves).

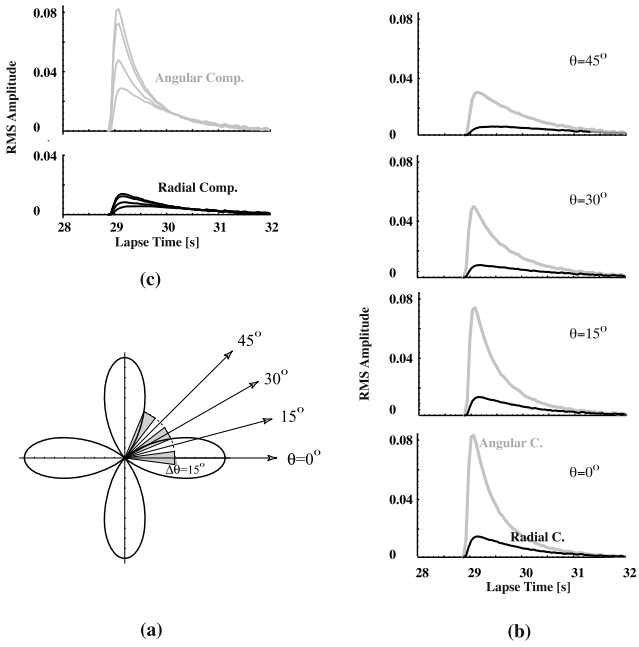

Fig. 9. Square root intensity envelopes at a distance of 100 km for a point shear dislocation S-source in 2-D random elastic media characterized by a Gaussian ACF based on the stochastic ray path method: (a) Radiation pattern of S-wave intensity; (b) Square root intensity envelopes at difference azimuths; (c) Square root intensity envelopes in the radial component (solid curves) and the angular component (gray curves).

obtained with the wandering term as given by Eqs. (12) and (16).

3.3 Coincidence of two vector envelope simulations for isotropic source radiation

For the synthesis of vector-wave envelopes for radiation from a point source, we shoot many particles from the origin and calculate the travel time distribution at a given radial distance and a ray coordinate angle θ. The Monte Carlo method is used to realize the ray bending process of each particle in each cylindrical layer. Here we synthesize vector envelopes in random elastic media characterized by a Gaussian ACF with $\varepsilon = 5\%$ and $a = 5$ km and mean P- and S-wave velocities of 6 km/s, and 3.46 km/s, respectively, where the number of shots is 100,000 and $\Delta r = 2$ km. Figure 7 shows the distribution of ray coordinate angle θ and that of local ray angle ϕ; this distribution means that the ASF spreads with increasing travel distance for the P-waves, where the initial ray direction is $\theta = 0$ and $\phi = 0$.

For the case of isotropic source radiation, we use a convolution of the resultant intensity and the uniform ray coordinate angle distribution. The thin black curves having small zigzag fluctuations in Figs. 8(a) and (b) show square root intensities calculated from the stochastic ray path method at a distance of 100 km from the P-wave source and S-wave source, respectively. The apparent duration of the S-wavelet is larger than that of P-wavelet. We plot corresponding solutions derived from the Markov approximation for TFMCF for comparison; these are shown as bold gray curves in Figs. 8(a) and (b). We find a good agreement between vector envelopes derived from the stochastic ray path method and those derived from the Markov approximation for TFMCF for the case of isotropic radiation from a point source. The coincidence of two methods for scalar wave case in 3-D was shown by Williamson (1972).

3.4 Vector wave envelopes for the case of a point shear dislocation source

The stochastic ray path method was originally developed for the case of isotropic source radiation; however, the advantage of the stochastic ray path method is that it is directly applicable to nonisotropic source radiation. A point shear dislocation source is the most important nonisotropic source radiation in seismology. The radiation pattern of wave intensity in a plane perpendicular to the null axis is written by

$$\Psi(\theta) = 2\cos 2\theta, \tag{35}$$

where the normalization is $\int_0^{2\pi} \Psi(\theta)\, d\theta = 2\pi$. Its radiation pattern is shown in Fig. 9(a). We first calculate intensities at a distance of 100 km for a unidirectional radiation ($\theta = 0$) from the origin using the stochastic ray path method. The number of shots is 100,000 and $\Delta r = 2$ km. Taking a convolution of the source radiation pattern (Eq. (35)) and ASF $\breve{\Gamma}_\phi$ obtained with respect to angle θ, we obtain angular- and radial-component intensities at any azimuth for the point shear dislocation source, where the whole angle is divided into 24 segments ($\Delta\theta = 15^\circ$). Figure 9(b) shows the square root intensities at four different azimuths at a 100-km distance for the point shear dislocation source radiation of S-waves. The peak amplitude of the angular-component is the largest at $\theta = 0^\circ$ as expected. We find that the peak amplitude of the radial component is about 20% of that of the angular component at $\theta = 0^\circ$. We also find excitation of wave amplitudes in both the angular and radial components, even in the direction of the nodal plane of S-wave radiation: the peak amplitude of the angular component at $\theta = 45^\circ$ is about 35% of that at $\theta = 0^\circ$.

A peak delay from the onset and a smooth decay after the peak are common to envelopes in all azimuths. We find that the difference in amplitudes between the radial and angular components becomes smaller with the reduced time increasing at any angles. As shown in Fig. 9(c), wave amplitudes near the peak arrival well reflect the source radiation pattern, but the difference in amplitudes for different azimuths diminishes as the reduced time increases in both radial and angular components. These simulations give a possible explanation for the observed fact that high-frequency seismograms of local earthquakes are insensitive to the focal plane solution as compared with those in low frequencies. Observed departure from the double-couple radiation pattern at high frequencies can be explained by scattering due to medium inhomogeneity.

4. Summary and Discussion

For the direct envelope synthesis of cylindrical vector waves in 2-D random elastic media, we have introduced two methods for the case that the medium inhomogeneity is small and the wavelength is shorter than the correlation distance. Since wave conversion between P-and S-waves can be neglected, potential fields of P- and S-waves are independently governed by parabolic equations. The stochastic master equation for TFMCF of the potential field is derived using the Markov approximation. For the case of Gaussian ACF, taking the Fourier transform of the analytical solution of TFMCF, we have newly derived two-component wave envelopes. The resultant envelope of each component shows peak amplitude decay, peak delay from the onset, and envelope broadening with increasing distance. The envelope characteristics are independent of frequency, and they are well quantified by the statistical parameters and the distance. The excitation of amplitude in the angular component for P-waves and that in the radial component for S-waves are clear evidence of scattering effect. For P-waves, the ratio of the time integral of the square of the angular component amplitude trace to that of the square-sum of two component amplitudes with geometrical correction leads to the ratio of the MS fractional fluctuation to the correlation distance. It gives a convenient way to determine this ratio from envelope data.

We numerically studied vector wave propagation in 2-D random elastic media (mean P- and S-wave velocities of 6 km/s and 3.46 km/s, respectively) characterized by Gaussian ACF ($\varepsilon = 0.05$, $a = 5$ km) for an isotropic radiation of a 2-Hz P-wavelet by using FD simulations. At each travel distance, we take the square root of the ensemble average of the square of numerically simulated amplitude traces to calculate the RMS envelope trace of each component, which shows a good coincidence with that derived from the Markov approximation for TFMCF, with the exception of the coda portion.

We next introduced the stochastic ray path method, which jointly uses the Markov approximation for MCF of the potential field and ray travel times. We have numerically confirmed the coincidence of the Markov approximation for TFMCF and the stochastic ray path method for Gaussian ACF. The advantage of the stochastic ray path method is that it is directly applicable to nonisotropic source radiation. We simulated vector wave envelopes at different azimuths for the case of a point shear dislocation source radiation. A peak delay from the onset and a smooth decay after the peak are common to envelopes in all azimuths. The difference in amplitudes between the radial and angular components becomes smaller with increasing reduced time. Peak amplitudes well reflect the source radiation pattern, but the difference in amplitudes for different azimuths diminishes as reduced time increases in both radial and angular components. These results qualitatively explain the observed fact that higher frequency seismograms of local earthquakes become insensitive to the focal plane solution compared with lower frequency ones. When large angle scattering is negligible, this method is essentially extendable for more general types of random media and a 3-D case. We are currently seeking a way to simulate wave envelopes by using the Markov approximation for TFMCF for the nonisotropic source radiation case.

Acknowledgments. H. S. is supported by the grant for Scientific Research #17540389 from JSPS and the JNES open application project for enhancing the basis of nuclear safety. M. K. acknowledges support from the Deutsche Forschungs Gemeinschaft under contract KO-1068/5. Comments of Anatoly Petukhin and an anonymous reviewer were helpful for revising the manuscript.

References

Aki, K. and B. Chouet, Origin of coda waves: Source, attenuation and scattering effects, *J. Geophys. Res.*, **80**, 3322–3342, 1975.

Bal, G. and M. Moscoso, Polarization effects of seismic waves on the basis of radiative transport theory, *Geophys. J. Int.*, **142**, 571–585, 2000.

Fehler, M., H. Sato, and L.-J. Huang, Envelope broadening of outgoing waves in 2-D random media: A comparison between the Markov approximation and numerical simulations, *Bull. Seismol. Soc. Am.*, **90**, 914–928, 2000.

Frankel, A. and R. W. Clayton, Finite difference simulations of seismic scattering: Implications for the propagation of short-period seismic waves in the crust and models of crustal heterogeneity, *J. Geophys. Res.*, **91**, 6465–6489, 1986.

Gusev, A. A. and I. R. Abubakirov, Simulated envelopes of non-isotropically scattered body waves as compared to observed ones: Another manifestation of fractal heterogeneity, *Geophys. J. Int.*, **127**, 49–60, 1996.

Hoshiba, M., Simulation of coda wave envelope in depth dependent scattering and absorption structure, *Geophys. Res. Lett.*, **21**, 2853–2856, 1994.

Ishimaru, A., *Wave Propagation and Scattering in Random Media*, vols. 1 and 2, Academic, San Diego, Calif., 1978.

Korn, M. and H. Sato, Synthesis of plane vector wave envelopes in two-dimensional random elastic media based on the Markov approximation and comparison with finite-difference simulations, *Geophys. J. Int.*, **161**, 839–848, 2005.

Lee, L. C. and J. R. Jokipii, Strong scintillations in astrophysics. I. The Markov approximation, its validity and application to angular broadening, *Astrophys. J.*, **196**, 695–707, 1975.

Margerin, L., M. Campillo, and B. Van Tiggelen, Monte Carlo simulation of multiple scattering of elastic waves, *J. Geophys. Res.*, **105**, 7873–7892, DOI:10.1029/1999JB900359, 2000.

Matsumura, S., Three-dimensional expression of seismic particle motions by the trajectory ellipsoid and its application to the seismic data observed in the Kanto district, Japan, *J. Phys. Earth*, **29**, 221–239, 1981.

Morse, P. M. and H. Feshbach, *Methods in Theoretical Physics*, McGraw-Hill, Boston, 1953.

Nakahara, H., T. Nishimura, H. Sato, and M. Ohtake, Seismogram envelope inversion for the spatial distribution of high-frequency energy radiation from the earthquake fault: Application to the 1994 far east off Sanriku earthquake, Japan, *J. Geophys. Res.*, **103**, 855–867, 1998.

Obara, K. and H. Sato, Regional differences of random inhomogeneities around the volcanic front in the Kanto-Tokai area, Japan, revealed from the broadening of S wave seismogram envelopes, *J. Geophys. Res.*, **100**,

2103–2121, 1995.

Petukhin, A. G. and A. A. Gusev, The Duration-distance relationship and average envelope shapes of small Kamchatka earthquakes, *Pure Appl. Geophys.*, **160**, 1717–1743, 2002.

Przybilla, J., M. Korn, and U. Wegler, Radiative transfer of elastic waves versus finite difference simulations in 2D random media, *J. Geophys. Res.*, **111**, B04305, doi:10.1029/2005JB003952, 2006.

Saito, T., H. Sato, and M. Ohtake, Envelope broadening of spherically outgoing waves in three-dimensional random media having power-law spectra, *J. Geophys. Res.*, **107**, doi: 10.1029/2001JB000264, 2002.

Saito, T., H. Sato, and M. Ohtake, Envelope broadening of spherically outgoing waves in three-dimensional random media having power-law spectra, *J. Geophys. Res.*, **107**, doi: 10.1029/2001JB000264, 2002.

Sato, H., Energy propagation including scattering effect: Single isotropic scattering approximation, *J. Phys. Earth*, **25**, 27–41, 1977.

Sato, H., Attenuation and envelope formation of three-component seismograms of small local earthquakes in randomly inhomogeneous lithosphere, *J. Geophys. Res.*, **89**, 1221–1241, 1984.

Sato, H., Broadening of seismogram envelopes in the randomly inhomogeneous lithosphere based on the parabolic approximation: Southeastern Honshu, Japan, *J. Geophys. Res.*, **94**, 17735–17747, 1989.

Sato, H. Synthesis of vector-wave envelopes in 3-D random elastic media characterized by a Gaussian autocorrelation function based on the Markov approximation: Plane wave case, *J. Geophys. Res.*, **111**, B06306, doi:10.1029/2005JB004036, 2006.

Sato, H., Synthesis of vector-wave envelopes in 3-D random elastic media characterized by a Gaussian autocorrelation function based on the Markov approximation: Spherical wave case, *J. Geophys. Res.*, **112**, B01301, doi:10.1029/2006JB004437, 2007.

Sato, H. and M. Fehler, "Seismic wave propagation and scattering in the heterogeneous earth", AIP Press/Springer Verlag New York, 1–308, 1998.

Scherbaum, F. and H. Sato, Inversion of full seismogram envelopes based on the parabolic approximation: Estimation of randomness and attenuation in southeast Honshu, Japan, *J. Geophys. Res.*, **96**, 2223–2232, 1991.

Shishov, V. L., Effect of refraction on scintillation characteristics and average pulsars, *Sov. Astron.*, **17**, 598–602, 1974.

Sreenivasiah, I., A. Ishimaru, and S. T. Hong, Two-frequency mutual coherence function and pulse propagation in a random medium: An analytic solution to the plane wave case, *Radio Sci.*, **11**, 775–778, 1976.

Uscinski, J., *The Elements of Wave Propagation in Random Media*, McGraw-Hill, New York, 1977.

Wegler, U., M. Korn, and J. Przybilla, Modeling of full seismogram envelopes using radiative transfer theory with Born scattering coefficients, *Pure Appl. Geophys.*, **163**, 503–531, 2006.

Williamson, I. P., Pulse broadening due to multiple scattering in the interstellar medium, *Mon. Not. R. Astron. Soc.*, **157**, 55–71, 1972.

Williamson, I. P., The broadening of pulses due to multi-path propagation of radiation, *Proc. R. Soc. London. A.*, **342**, 131–147, 1975.

Yomogida, K. and R. Benites, Relation between direct wave and coda : A numerical approach, *Geophys. J. Int.*, **123**, 471–483, 1995.

Yoshimoto, K., Monte Carlo simulation of seismogram envelopes in scattering media, *J. Geophys. Res.*, **105**, 6153–6161, 2000.

Zeng, Y., K. Aki, and T. L. Teng, Mapping of the high-frequency source radiation for the Loma Prieta earthquake, California, *J. Geophys. Res.*, **98**, 11981–11993, 1993.

H. Sato (e-mail: sato@zisin.geophys.tohoku.ac.jp) and M. Korn